

3.2.1 OTSK1A

3.2.1-1 Atmospheric Correction for Ocean Color

A. Algorithm Outline

- (1) Algorithm name: Atmospheric Correction for Ocean Color
- (2) Product Code: NWLR
- (3) PI names: G-0065 Hajime Fukushima
- (4) Overview of algorithm (Status: Operational level)

This algorithm is an extension of the OCTS atmospheric correction algorithm (Fukushima et al., 1998).

It treated the multiple scattering among the aerosol particles and gas molecules, as well as the effects of variable ozone concentration, surface pressure, surface wind speed, and water vapor amount. The atmospheric correction with iterative procedure was developed to avoid the black pixel assumption. Due to saturation problems of the GLI nominal band16 (749nm) and band18 (865nm), alternative bands (band13:678nm and band19:865nm) were used. The water reflectance at near infrared bands are estimated by in-water model for chlorophyll a (chl) and inorganic suspended matter (ism) concentrations as well as absorption coefficient of colored dissolved organic matter (cdom). These values are estimated by using a neural network-based in-water algorithm.

B. Theoretical Description

- (1) Methodology and Logic flow

1-1 Radiative transfer model

The satellite-observed reflectance, ρ_T , is modeled as follows.

$$\rho_T(\lambda) = \rho_M(\lambda) + \rho_A(\lambda) + \rho_{MA}(\lambda) + T(\lambda)\rho_G(\lambda) + t(\lambda)\rho_{WC}(\lambda) + t(\lambda)\rho_W(\lambda) \quad (1)$$

where λ is wavelength, ρ_M is reflectance due to gas molecules, ρ_A is aerosol reflectance, ρ_{MA} is reflectance due to the interaction between molecules and aerosol particles, ρ_G is the reflectance resulting from the specular reflection by the direct sun light, ρ_{WC} is the reflectance resulting from the whitecap, ρ_W is reflectance of the ocean, T is the direct transmittance of the atmosphere, and t is the diffuse transmittance of the atmosphere.

The ρ_G term in the above equation is generally ignored because ocean-color sensors are equipped with a provision for tilting the scan plane away from the specular image of the sun. The purpose of atmospheric correction is to retrieve ρ_W from above equation with ρ_M which is calculated based on the lookup tables and $\rho_A + \rho_{MA}$ and t which are estimated by the satellite data.

1-2 Aerosol models

Since the water reflectance, ρ_W , can be discarded in the NIR (710~865nm) bands, we obtain the aerosol reflectance for these bands including the interaction part as follows,

$$\rho_A(\lambda) + \rho_{MA}(\lambda) = \rho_T(\lambda) - \rho_M(\lambda) \quad (2)$$

We need to estimate $\rho_A + \rho_{MA}$ for band 1 to 12 and 14 but it is not straight forward since the spectral relation of $\rho_A + \rho_{MA}$ over the whole visible and near IR region is dependent on θ_0 , θ , the satellite zenith angle, and $\Delta\phi$, the relative azimuth angle between the sun and the satellite, in addition to the type and optical thickness of aerosol. Similar to the method proposed by Gordon and Wang (1994), we introduce the tables that store the relation between the aerosol reflectance $\rho_A + \rho_{MA}$ and aerosol optical thickness, τ_A , for each band and use them to determine the magnitude of $\rho_A + \rho_{MA}$ in the shorter wavelengths bands based

on the estimated spectral ratio of ϵ between two NIR bands. Since the relation between $\rho_A + \rho_{MA}$ and τ_A is dependent on aerosol type, GLI algorithm has the following nine candidate aerosol models:

- Tropospheric aerosol with R.H. of 70% (Model 1)
- Oceanic1600 aerosol with R.H. of 70% (Model 2)
- Oceanic800 aerosol with R.H. of 70% (Model 3)
- Oceanic400 aerosol with R.H. of 70% (Model 4)
- Oceanic200 aerosol with R.H. of 60 and 73% (Models 5 and 6)
- Oceanic100 aerosol with R.H. of 70% (Model 7)
- Oceanic50 aerosol with R.H. of 70 and 83% (Model 8 and 9)

The definition of these models are based on Shettle and Fenn (1979). The “Oceanic1600 type” consists of 99.9375% (one 1600th) of tropospheric and 0.0625% of oceanic aerosols, in terms of number of particles. RH means the assumed relative humidity. Other models through Model 9 are defined similarly.

1-3 Lookup tables

The following lookup tables were prepared beforehand to speed up processing of atmospheric correction.

- ρ_M table that gives $\rho_M(\lambda)$ for the given θ_0 , θ , and $\Delta\phi$.

- “ $\rho_A + \rho_{MA} \rightarrow \tau_A$ ” table that contains coefficients a_0 , a_1 , a_2 , a_3 and a_4 in the equation,

$$\begin{aligned} \tau_A(\lambda) &= a_0 + a_1 X(\lambda) + a_2 X(\lambda)^2 + a_3 X(\lambda)^3 + a_4 X(\lambda)^4 \\ X(\lambda) &= \rho_A(\lambda) + \rho_{MA}(\lambda) \end{aligned} \quad (3)$$

for all $(\theta_0, \theta, \Delta\phi)$, aerosol types and atmospheric correction bands such as 678nm (ch13), 749nm (ch16), 865nm (ch18) and 865nm (ch19, denoted as 865A band).

- “ $\tau_A \rightarrow \rho_A + \rho_{MA}$ ” table that contains coefficients a_0 , a_1 , a_2 , a_3 and a_4 in the equation,

$$\rho_A(\lambda) + \rho_{MA}(\lambda) = a_0 + a_1 \tau_A(\lambda) + a_2 \tau_A(\lambda)^2 + a_3 \tau_A(\lambda)^3 + a_4 \tau_A(\lambda)^4 \quad (4)$$

for all $(\theta_0, \theta, \Delta\phi)$, aerosol types and channels except atmospheric correction bands..

- ω_A table that has the single scattering albedo of all the aerosol models.

- K_{EXT} table that contains the values of extinction coefficients for all aerosol models.

- P_A table that retains aerosol scattering phase functions for all the aerosol models.

The entries for these tables were all generated by rstar5b code developed by T. Nakajima and his group.

1-4 Saturation problem at 749nm and 865nm bands

It has been predicted that 749nm and 865nm bands will be saturated even in the fair-sky oceans. Some numerical simulations on atmospheric correction have been conducted in order to investigate alternative atmospheric correction bands. The analysis revealed that 678nm (ch13) and 865nm (ch19) bands could be used as the alternative bands. Therefore two band pairs, i.e. 749nm and 865nm band pair and 678nm and 865nm (ch19, "865A") band pair, are alternatively used as the atmospheric correction bands. Pixel-wise-procedure of GLI atmospheric correction algorithm with the alternative bands will be described in the next section.

1-5 Pixel-wise procedure

The pixel-wise procedure for the atmospheric correction is described as follows. In what follows, $\varepsilon'(M)$ means the estimated value of the spectral ratio of $\omega_A \tau_A P_A$ between 749 and 865nm bands for an assumed aerosol model M, while $\varepsilon(M)$ is the theoretically derived value of $\omega_A K_{EXT} P_A$ ratio for a model M. And 865A means 865nm (ch19).

An annotated flow diagram of the entire atmospheric correction algorithm is presented in Fig.1.

- (a) Convert total radiance, L_T , into total reflectance, ρ_T .
- (b) Calculate white cap reflectance, ρ_{WC} .
- (c) Calculate air molecules scattering reflectance, ρ_M , by using lookup tables.
- (d) Subtract ρ_M and ρ_{WC} from $\rho_T(\lambda)$.
- (e) When measured radiance at 749nm band, $L_t(749)$, is less than 0.9 mW/cm²/μm/sr and $L_t(865)$ is less than 0.6 mW/cm²/μm/sr, estimate τ_A at 749nm and 865nm bands for each candidate aerosol model(M) in reference to the aerosol lookup tables. Then proceed to step (i).
- (f) When $L_t(749)$ is in the range of 0.9 - 1.2 mW/cm²/μm/sr estimate τ_A at 678nm and 749nm band for each candidate aerosol model(M) in reference to the aerosol lookup tables, and convert $\tau_A(M, 678)$ to $\tau_A'(M, 749)$ by using K_{ext} lookup tables. Then $\tau_A(M, 749)$ and $\tau_A'(M, 749)$ are composed as follows:

$$\tau_A(M, 749) = \text{ratio1} * \tau_A(M, 749) + (1 - \text{ratio1}) * \tau_A'(M, 749) \quad (5)$$

$$\text{ratio1} = -30.0 + (240.0 + (-233.0 + 74.0741 * L_t(749)) * L_t(749)) * L_t(749) \quad (6)$$
- (g) When $L_t(865)$ is in the range of 0.6 - 0.8 mW/cm²/μm/sr, estimate τ_A at 865nm and 865A bands for each candidate aerosol model(M) in reference to the aerosol lookup tables, and convert $\tau_A(M, 865A)$ to $\tau_A'(M, 865)$ by using K_{ext} lookup tables. Then $\tau_A(M, 865)$ and $\tau_A'(M, 865)$ are composed as follows:

$$\tau_A(M, 865) = \text{ratio2} * \tau_A(M, 865) + (1 - \text{ratio2}) * \tau_A'(M, 865) \quad (7)$$

$$\text{ratio2} = -30.0 + (360.0 + (-525.0 + 250.000 * L_t(865)) * L_t(865)) * L_t(865) \quad (8)$$
- (h) When $L_t(749)$ and $L_t(865)$ are over 1.2 and 0.8 mW/cm²/μm/sr, respectively, estimate τ_A at 678nm and 865A bands for each candidate aerosol model(M) in reference to the aerosol lookup tables. Then convert $\tau_A(M, 678)$ and $\tau_A(M, 865A)$ to $\tau_A(M, 749)$ and $\tau_A(M, 865)$ by using K_{ext} lookup tables, respectively.
- (i) Calculate ε' value for 9 aerosol models at 749nm and 865nm bands.

$$\begin{aligned} \varepsilon'(M, 749, 865) &= \frac{\rho_{AS}(749)}{\rho_{AS}(865)} \\ &= \frac{\omega_A(M, 749) \tau_A(M, 749) P_A(M, 749)}{\omega_A(M, 85) \tau_A(M, 865) P_A(M, 865)} \end{aligned} \quad (9)$$

- (i) Calculate ε'_{ave} and select a pair of aerosol models A and B, such that $\varepsilon(A) < \varepsilon'_{ave}$ and $\varepsilon(B) > \varepsilon'_{ave}$, by the iteration scheme. Define interpolation ratio r as $(\varepsilon'_{ave} - (\varepsilon(A))) / ((\varepsilon(B)) - (\varepsilon(A)))$.

(j) For models A and B, obtain $A(\lambda, M)$ for band 1 to 12 and 14 by

$$\tau_A(\lambda, M) = \frac{K_{ext}(\lambda, M)}{K_{ext}(865, M)} \tau_A(865, M) \quad (10)$$

Derive $\rho_A(\lambda) + \rho_{MA}(\lambda)$ for the models A and B in use of the aerosol lookup tables.

(k) Obtain final $\rho_A(\lambda) + \rho_{MA}(\lambda)$ by interpolating the $\rho_A + \rho_{MA}$ values for the models A and B.

(l) Calculate water-leaving reflectance, ρ_w .

(m) Convert ρ_w into normalized water-leaving radiance, nL_w .

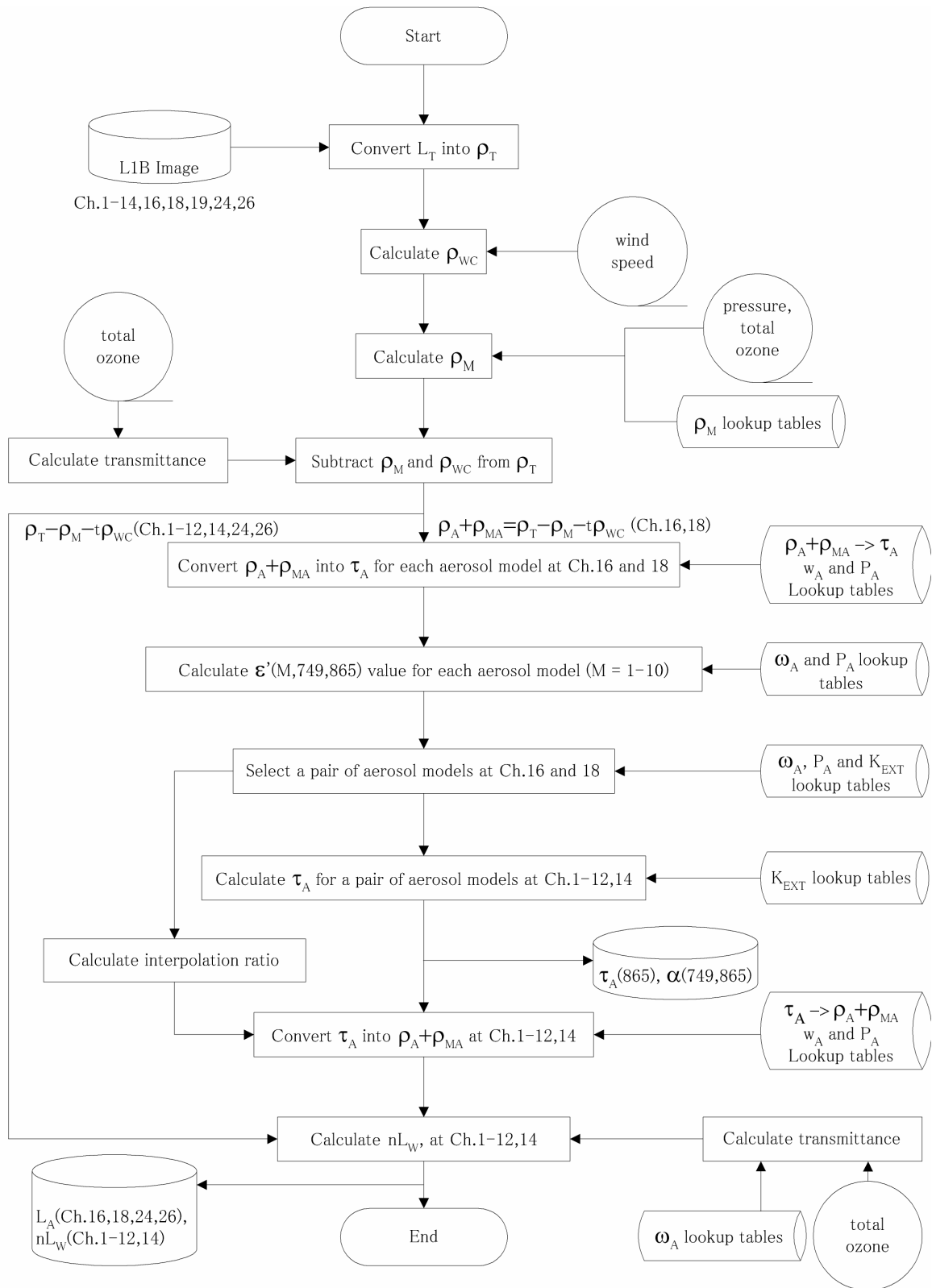


Fig.1 An annotated flow diagram of the pixel-wise GLI atmospheric correction

1-6 Atmospheric correction with iteration (new OTSK1)

Due to saturation problems of the GLI nominal band16 (749nm) and band18 (865nm) even in non-cloudy ocean areas, GLI band13 (678nm) and band19 (865nm), were used for atmospheric correction. An iteration scheme is needed since these bands may be influenced by upward radiance from the sea. These near-infrared (NIR) water-leaving radiances should be corrected before atmospheric correction by using specific in-water model.

We developed an iterative procedure that corrects atmospheric effect with iteration to avoid the black pixel assumption (Siegel et al., 2000). As shown in Figure 3-1, the water reflectance at near infrared bands are first estimated by using in-water model assuming initial values for chlorophyll a (chl) and inorganic suspended matter (ism) concentrations as well as absorption coefficient of colored dissolved organic matter (cdom). First atmospheric correction is executed, and new chl, ism and cdom are estimated by using neural network in-water algorithm. After the first atmospheric correction, the new water-leaving reflectance is estimated from obtained chl, and the second stage atmospheric correction is conducted. This process is repeated until chl, ism and cdom estimates converge.

1-6-1 In-water model at near infrared region

The in-water model for NIR water-leaving radiance is defined as follows

$$[\rho_w(\lambda)]_N = 0.533\pi R(\lambda)/Q, \quad (11)$$

by Lee et al. (1994) where λ is wavelength, and $Q = 4.5$ (Morel and Gentili, 1991). $[\rho_w(\lambda)]_N$ is normalized water-reflectance (Gordon, 1997) given by

$$[\rho_w(\lambda)]_N = \rho_w(\lambda)/t_0, \quad (12)$$

where t_0 is the transmittance between sun and ocean surface. R is the reflectance just below surface and is defined by Joseph (1950) as

$$R(\lambda) = \frac{\sqrt{1 + 2b_b(\lambda)/a(\lambda)} - 1}{\sqrt{1 + 2b_b(\lambda)/a(\lambda)} + 1} \quad (13)$$

where a and b_b is absorption and backward scattering coefficient, respectively. $a(\lambda)$ and $b_b(\lambda)$ are defined by

$$a(\lambda) = a_w(\lambda) + a_c(\lambda, chl) + a_s(\lambda, ism) + a_y(\lambda), \quad (14)$$

and

$$b_b(\lambda) = b_{bw}(\lambda) + b_{bc}(\lambda, chl) + 2.7 \cdot b_{bs}(\lambda, ism) \quad (15)$$

where subscript w, c, s, y represents water, chlorophyll-a, inorganic suspended matter and yellow substance (cdom) respectively. Absorption coefficient values are given as follows.

$$a_w(678) = 0.42829, \quad a_w(865) = 4.6416 \quad (16)$$

by Pope and Fry (1997)

$$a_c(\lambda) = a_{cs}(\lambda) \cdot chl \quad (17)$$

where chl is chlorophyll a concentration in mg/m^3

$$a_{cs}(678) = 0.01968, \quad a_{cs}(865) = 0 \quad \text{by Kishino (personal comm.)} \quad (18)$$

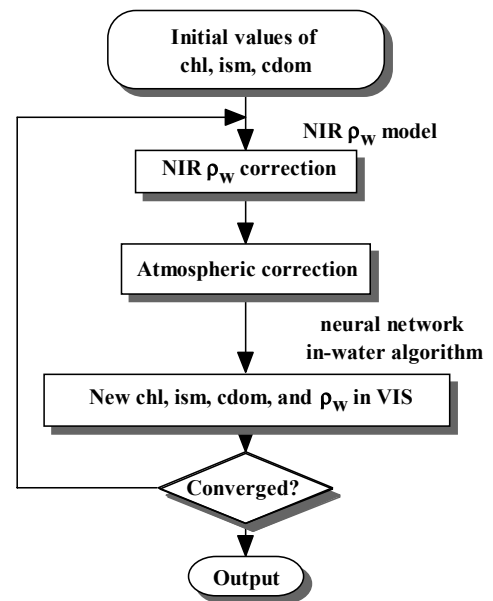


Figure 3-1 A simplified flow diagram of the pixel-wise GLI atmospheric correction with iteration. In the diagram, NIR and VIS stand for the near-infrared and visible bands, respectively.

$$a_y(\lambda) = a_y(440) \cdot \exp\{-0.014 \cdot (\lambda - 440)\} \quad \text{by Bricaud et al. (1981)} \quad (19)$$

The back scattering coefficients are given as follows:

$$b_{bw}(\lambda) = 0.5 \times 0.00288 \cdot \left(\frac{\lambda}{550}\right)^{-4.32} \quad \text{by Morel (1974)} \quad (20)$$

$$b_{bc}(\lambda) = 0.081 \cdot b_c(\lambda) \quad \text{by Oishi et al. (2002)} \quad (21)$$

$$b_c(\lambda) = 0.27 \cdot chl^{0.698} \cdot \left(\frac{\lambda}{550}\right)^{-0.2933} \quad \text{by Kishino (personal comm..)} \quad (22)$$

$$b_{bs}(\lambda) = b_s(\lambda) \cdot 0.01478 \quad \text{by Babin and Doerffer (1996)} \quad (23)$$

$$b_s(\lambda) = 0.125 \cdot ism \cdot \left(\frac{\lambda}{550}\right)^{-0.812} \quad \text{by Kronfeld (1988)} \quad (24)$$

1-6-2 Neural network-based in-water algorithm

A neural network is used for the iteration process to derive estimates of the chlorophyll-a concentration (chl), inorganic suspended solid concentration (ism) and absorption coefficient of colored dissolved organic matter (cdom) at 440nm (Tanaka et al., 1998). The inputs for the neural net are the normalized water-leaving radiances at 412, 443, 460, 520, and 545 nm bands. These bands are chosen because they have high saturation radiances.

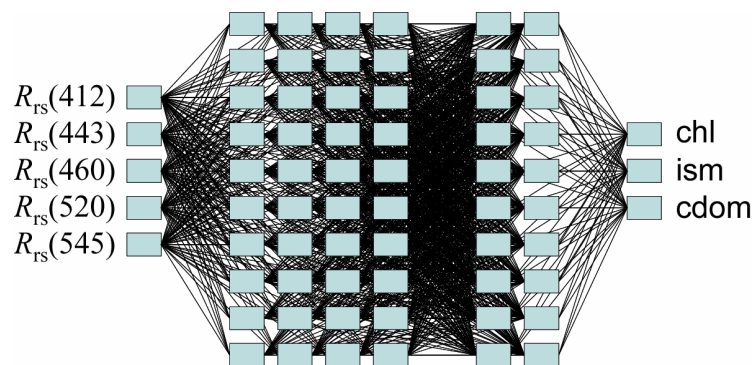


Figure 3-2 Neural network-based in-water algorithm

1-6-3 Alternative bands

Due to saturation problems of the GLI nominal band16 (749nm) and band18 (865nm) even in non-cloudy ocean areas, GLI band13 (678nm) and band19 (865nm), were used for atmospheric correction. An iteration scheme is needed since these bands may be influenced by upward radiance from the sea. These near-infrared (NIR) water-leaving radiance should be corrected before atmospheric correction by using specific in-water model.

(2) Physical and Mathematical aspects of the algorithm

This algorithm is originated from the Ocean Color Atmospheric Correction algorithm. An extension from the OCTS algorithm is being made to improve the processing accuracies by taking use of many additional and new GLI bands. The OCTS algorithm, in turn, was initially developed based on an atmospheric correction method used to handle SeaWiFS data (Gordon and Wang, 1994), in taking the following effects into consideration:

- Polarized Rayleigh scattering (including the multiple scattering)
- Aerosol scattering
- Scattering among aerosol particles and gas molecules
- Reflection of sky light from sea surface
- Absorption effect by ozone
- Transmittance along the path sun-to-sea surface-to-satellite
- Sun glint

Corrections of the light components due to Rayleigh scattering and aerosol scattering etc. are made by using lookup tables prepared beforehand. In addition to the atmospheric pressure, ozone concentration, wind speed etc., the atmospheric correction requires also other kinds of analysis data made available by Meteorological Agency.

When applying to GLI, the following effects will be newly taken into account:

- Influence of white cap
- Absorbing effect of water vapor
- Absorbing effects of carbon dioxide gas and others

C. References

1. Research Report: On the development of a retrieval algorithm for ADEOS-II/GLI ocean color data – Chapter 3: An Algorithm for GLI Ocean Color Atmospheric Correction, FY1996.
2. Research Report: Advanced Earth Observing Satellite (ADEOS) OCTS Data Processing Algorithm Description Ver.2.0 (NASDA) – Chapter 8.6: OCTS Type Algorithm.
3. Babin M. and R. Doerffer (1996), Specifications for case II coastal water reference model., Algorithm Theoretical Basis Document for MERIS (ATBD 2.12), ESA-ESTEC, pp.61-73.
4. Bricaud, A.,A. Morel and L. Prieur(1981), Absorption by dissolved organic matter of the sea (yellow substance) in the UV and visible domains, *Limnol. Oceanogr.*, Vol.26, No.1, pp.43-53.
5. Ding, K. Y., & Gordon, H. R. (1994). Atmospheric correction of ocean color sensors: Effects of the earth's curvature. *Applied Optics*, 33 (30), 7096-7106.
6. Fukushima, H. A. Higurashi, Y. Mitomi, T. Nakajima, T. Noguchi, T. Tanaka, and M. Toratani (1998): Correction of atmospheric effect on ADEOS/OCTS ocean color data: Algorithm description and evaluation of its performance, *J. Oceanography*, 54, 417-430.
7. Fukushima, H. and M. Toratani (1997): Asian dust aerosol: optical effect on satellite ocean color signal and a scheme of its correction. *J. Geophys. Res.*, 102(D14), 17,119-17,130
8. Gordon, H.R.(1997),Atmospheric correction of ocean color imagery in the Earth Observation System era, *J. Geophys. Res.*, 102 (D14), 17,081-17,106.
9. Gordon, H.R., and M. Wang.(1994), Retrieval of water-leaving radiance and aerosol optical thickness over the oceans with SeaWiFS: a preliminary algorithm, *Appl. Opt.*, 33 (3), 443-452.
10. Joseph, J. (1950), Untersuchungen über ober- und unterlichtmessungen im Meere und über ihren

- zusammenhang mit durchsichtigkeitsmessungen, Deut. Hydorograph. Z., Vol.3, pp.324-335.
11. Kronfeld, U. (1988), Die optischen Eigenschaften der ozeanischen Schwebstoffe und ihre Bedeutung für die Fernerkundung von Phytoplankton., GKSS Forschungszentrum, D-2054 Geesthacht, Germany, p.153.
 12. Lee, Z., K. Carder, S. Hawes, R. Steward, T. Peacock and C. Davis (1994), Model for the interpretation of hyperspectral remote-sensing reflectance, *Applied Optics*, Vol.33, pp.5721-5732.
 13. Morel A. and B. Gentili (1991), Diffuse reflectance of oceanic waters: its dependence on sun angle as influenced by the molecular scattering contribution, *Applied Optics*, 30, 4427-4438.
 14. Morel, A. (1974), Optical properties of pure water and pure sea water, chapter 1 in *Optical Aspects of Oceanography*, edited by N. G. Jerrov and E.S. Nielsen, Academic Press, New York, 1-24.
 15. Nakajima, T., M. Tanaka, M. Yamamoto, M. Shiobara, K. Arao, and Y. Nakanishi (1989), Aerosol optical characteristics in the yellow sand events observed in May, 1982 at Nagasaki - part II models, *J. Meteor. Soc. Japan*, 67, 279-291.
 16. Oishi, T., Y. Takahashi, A. Tanaka, M. Kishino, and A. Tsuchiya (2002), Relation between the backward- as well as total scattering coefficients and the volume scattering functions by cultured phytoplankton. *J. School Mar. Sci. Technol. Tokai Univ.*, Vol.53, pp.1-15 (in Japanese with English abstract).
 17. Pope, R. M. and E. S. Fry (1997), Absorption spectrum (380-700) of pure water, II: Integrating cavity measurement, *Applied Optics*, Vol.36, pp.8710-8723.
 18. Shettle, E.P., and R. W. Fenn. (1979), Models for the aerosols of the lower atmosphere and the effects of humidity variations on their optical properties, AFGL-TR-79-0214, 675, 94pp.,
 19. Siegel D. A., M. Wang, S. Maritorena, and W. Robinson (2000): Atmospheric correction of satellite ocean color imagery: the black pixel assumption, *Appl. Opt.*, 30, 21, 3582-3591.
 20. Tanaka, A., T. Oishi, M. Kishino, and R. Doerffer (1998), "Application of the neural network to OCTS data", *Proc. Ocean Optics XIV*, S. G. Ackleson and J. Campbell (eds.), Office of Naval Research, Washington, D.C..

3.2.1-2 Algorithm to estimate daily Photo-synthetically Available Radiation at the Ocean surface (OTSK14)

A. Algorithm Outline

- (1) Algorithm name: Daily Photo-synthetically Available Radiation at the Ocean surface (OTSK14)
- (2) Product Code: PAR
- (3) PI names: G-0035 Robert Frouin
- (4) Overview of algorithm (Status: Operational level)

The algorithm estimates daily (i.e., 24-hour averaged) Photo-synthetically Active Radiation (PAR) reaching the ocean surface.

B. Theoretical Description

PAR is defined as the quantum energy flux from the Sun in the spectral range 400-700 nm. It is expressed in Einstein/m²/day.

The PAR model uses plane-parallel theory and assumes that the effects of clouds and clear atmosphere can be de-coupled. The planetary atmosphere is therefore modeled as a clear sky atmosphere positioned above a cloud layer. This approach was shown to be valid by Dedieu et al. (1987) and Frouin and Chertock (1992). The great strength of such a de-coupled model is its simplicity. It is unnecessary to distinguish between clear and cloudy regions within a pixel, and this dismisses the need for often-arbitrary assumptions about cloudiness distribution.

Under solar incidence θ_s , the incoming solar flux at the top of the atmosphere, $E_0 \cos(\theta_s)$ is diminished by a factor $T_d T_g / (1 - S_a A)$ by the time it enters the cloud/surface layer. In this expression, T_d is the clear sky diffuse transmittance, T_g is the gaseous transmittance, S_a is the spherical albedo, and A is the cloud/surface layer albedo. As the flux, $E_0 \cos(\theta_s) T_d T_g / (1 - S_a A)$, passes through the cloud/surface layer, it is further reduced by a factor A . The solar flux reaching the ocean surface is then given by

$$E = E_{clear} (1 - A) (1 - A_s)^{-1} (1 - S_a A)^{-1} \quad (1)$$

where A_s is the albedo of the ocean surface and $E_{clear} = E_0 \cos(\theta_s) T_d T_g$ is the solar flux that would reach the surface if the cloud/surface layer were non reflecting and non-absorbing. In clear sky conditions, A reduces to A_s .

In order to compute E , A is expressed as a function of the radiance measured by GLI in the PAR spectral range. The algorithm works pixel by pixel and proceeds as follows.

First, for each pixel not contaminated by glitter the GLI radiance L_i^* in band i ($i = 1, 2, \dots, 6$), where 1 is 0.412 μm , 2 is 0.443 μm , 3 is 0.490 μm , 4 is 0.519 μm , 5 is 0.544 μm , and 6 is 0.679 μm , expressed in $\text{mW}/\text{cm}^2/\mu\text{m}/\text{sr}$, is transformed into reflectance, R_i^* :

$$R_i^* = \pi L_i^* / [E_{0i} (d_0/d)^2 \cos(\theta_s^*)] \quad (2)$$

where E_{0i} is the extra-terrestrial solar irradiance in band i , θ_s^* is the sun zenith angle at the GLI observation time, and d_0/d is the ratio of mean and actual Earth-Sun distance. The glint areas are not selected because they would be interpreted as cloudy in the PAR algorithm.

Second, R_i^* is corrected for gaseous absorption, essentially due to ozone:

$$R_i' = R_i^* / T_{gi} \quad (3)$$

with

$$T_{gi} = \exp[-k_i U / \cos(\theta_s^*)] \quad (4)$$

where k_i is the ozone absorption coefficient in band i and U the ozone amount.

Third, the reflectance of the cloud/surface layer, R_i , is obtained from R_i' following Tanré et al. (1979) and assuming isotropy of the cloud/surface layer system. That is:

$$R_i = (R_i' - R_{ai}) [T_{di}(\theta_s^*) T_{di}(\theta_v) + S_{ai} (R_i' - R_{ai})]^{-1} \quad (5)$$

where θ_v is the viewing zenith angle and R_{ai} is the intrinsic atmospheric reflectance in band i (corresponds to photons that have not interacted with the cloud/surface layer). The assumption of isotropy is made because no information on pixel composition is available.

In Eq. (5), R_a is modeled using the quasi single-scattering approximation:

$$R_a = (\tau_{mol}P_{mol} + \omega_{aer}\tau_{aer}P_{aer})[4\cos(\theta_s^*)\cos(\theta_v)]^{-1} \quad (6)$$

where τ_{mol} and τ_{aer} are the optical thicknesses of molecules and aerosols, P_{mol} and P_{aer} are their respective phase functions, and ω_{aer} is the single scattering albedo of aerosols. Subscript i has been dropped for clarity. The diffuse transmittance T_d and spherical albedo S_a are computed using analytical formulas developed by Tanré et al. (1979):

$$T_d(\theta) = \exp[-(\tau_{mol} + \tau_{aer})/\cos(\theta)]\exp[(0.52\tau_{mol} + 0.83\tau_{aer})/\cos(\theta)] \quad (7)$$

$$S_a = (0.92\tau_{mol} + 0.33\tau_{aer})\exp[-(\tau_{mol} + \tau_{aer})] \quad (8)$$

where θ is either θ_s^* or θ_v .

The optical thickness of aerosols in band i , τ_{aeri} , is obtained from the optical thickness in band 18 centered at 0.866 μm , τ_{aer18} , and the Angström coefficient, α :

$$\tau_{aeri} = \tau_{aer18}(\lambda_{18}/\lambda_i)^\alpha \quad (9)$$

where λ_i and λ_{18} are equivalent wavelengths in GLI bands i and 18, respectively. A monthly climatology may be used for τ_{aer} and α , since aerosol properties cannot be determined when the pixel is cloudy. This procedure is also justified because, in general, aerosol effects on E are secondary compared to cloud or θ_s effects.

To estimate ω_{aer} and P_{aer} , the two closest of 12 aerosol models, k and l , that verify $\alpha(l) < \alpha < \alpha(k)$ are selected, and a distance $d_{aer} = [\alpha(l) - \alpha]/[\alpha(l) - \alpha(k)]$ is computed. Using this distance, ω_{aer} and P_{aer} are obtained as follows:

$$\omega_{aer} = d_{aer}\omega_{aer}(k) + (1 - d_{aer})\omega_{aer}(l) \quad (10)$$

$$P_{aer} = d_{aer}P_{aer}(k) + (1 - d_{aer})P_{aer}(l) \quad (11)$$

where $\omega_{aer}(l)$ and $\omega_{aer}(k)$ are the single scattering albedos of aerosol models l and k , and $P_{aer}(l)$ and $P_{aer}(k)$ their respective phase functions.

Next, an estimate of daily PAR, $\langle E \rangle_{day}$, is obtained by integrating Eq. (1) over the length of the day:

$$\langle E \rangle_{day} = \langle E_0 \rangle \{ \cos(\theta_s) \langle T_g \rangle \langle T_d \rangle [1 - \langle A \rangle] [1 - \langle A_s \rangle]^{-1} [1 - \langle S_a \rangle \langle A \rangle]^{-1} \} dt \quad (12)$$

with

$$\langle T_g \rangle = \exp[-\langle k \rangle U / \cos(\theta_s)] \quad (13)$$

$$\langle T_d \rangle = \sum_i (T_{di} E_{oi}) / \sum_i E_{oi} \quad (14)$$

$$\langle S_a \rangle = \sum_i (S_{ai} E_{oi}) / \sum_i E_{oi} \quad (15)$$

$$\langle A_s \rangle = \langle T_{dir} \rangle \langle T_d \rangle^{-1} [0.05 / (1.1 [\cos(\theta_s)]^{1.4} + 0.15] + 0.08 \langle T_{dif} \rangle \langle T_d \rangle^{-1}] \quad (16)$$

$$\langle T_{dir} \rangle = \sum_i T_{diri} E_{oi} / \sum_i E_{oi} \quad (17)$$

$$\langle T_{dif} \rangle = \langle T_d \rangle - \langle T_{dir} \rangle \quad (18)$$

$$T_{diri} = \exp[-(\tau_{moli} + \tau_{aeri}) / \cos(\theta_s)] \quad (19)$$

$$\langle A \rangle = F \langle R(t^*) \rangle \quad (20)$$

$$\langle R \rangle = \sum_i R_i(t^*) / \sum_i E_{oi} \quad (21)$$

where t^* is the GLI observation time, T_{diri} is the direct component of T_{di} in band i , and $\langle \rangle$ symbolizes average value over the PAR range. Note that because of saturation at low radiance in some of the GLI spectral bands, the algorithm only takes into account, for each pixel, the spectral bands that do not saturate. It is possible, as an option, however, to use only the band centered at 0.679 μm (does not saturate over clouds) to estimate cloud effects on PAR. In the code, this option is activated when the flag "flag679" is on.

In Eq. (12), absorption by water vapor in the PAR spectral range, occurring weakly between 690 and 700 nm, is neglected. The ozone absorption coefficient $\langle k \rangle$ in Eq. (13) is taken from Frouin et al. (1989). Surface albedo is parameterized as a function of sun zenith angle and fractions of direct and diffuse incoming sunlight, according to Briegleb and Ramanathan (1982). This parameterization, which takes into account Fresnel reflection and diffuse under-light, is sufficient since the influence of $\langle A_s \rangle$ on surface PAR is small.

Even though the cloud/surface layer is assumed to be isotropic in the correction of clear atmosphere effects (Eq. 5), and therefore $A \approx R$, the dependence of A on sun zenith angle is taken into account via the angular factor, F (Eq. 20). Instead of using for F angular models determined statistically (e.g., Young et al., 1998), analytical formulas proposed by Zege (1991) for non-absorbing, optically thick scattering layers are applied. The available angular models are fairly similar for partly cloudy, mostly cloudy, and overcast conditions, and they compare reasonably well with Zege's (1991) formulas.

The cloud/surface layer, however, is assumed to be stable during the day and to correspond to the GLI observation. This assumption is crude, and PAR accuracy will be degraded in regions where clouds exhibit strong diurnal variability. Still, useful daily PAR estimates would be obtained by averaging in space and time. Note that using Eq. (12) the algorithm yields a daily PAR estimate for each instantaneous GLI pixel.

Finally, the individual daily PAR estimates, obtained in units of $\text{mW}/\text{cm}^2/\mu\text{m}$, are converted into units of $\text{Einstein}/\text{m}^2/\text{day}$. The factor required to convert units of $\text{mW}/\text{cm}^2/\mu\text{m}$ to units of $\text{Einstein}/\text{m}^2/\text{day}$ is equal to 1.193 to an inaccuracy of a few percent regardless of meteorological conditions (Kirk, 1994, pp. 4-8.). In middle and high latitudes, several daily estimates may be obtained over the same target during the same day, increasing product accuracy.

References

1. Briegleb, B. P., and V. Ramanathan, 1982: Spectral and diurnal variations in in clear sky planetary albedo. *J. Climate Appl. Meteor.*, **21**, 1168-1171.
2. Dedieu, G. P.-Y. Deschamps, and Y. H. Kerr, 1987: Satellite estimation of solar irradiance at the surface of the earth and of surface albedo using a physical model applied to Meteosat data. *J. Climate Appl. Meteor.*, **26**, 79-87.
3. Frouin, R., D. W. Lingner, K. Baker, C. Gautier, and R. Smith, 1989: A simple analytical formula to compute clear sky total and photosynthetically available solar irradiance at the ocean surface. *J. Geophys. Res.*, **94**, 9731-9742.
4. Frouin, R., and B. Chertock, 1992: A technique for global monitoring of net solar irradiance at the ocean surface. Part I: Model. *J. Appl. Meteor.*, **31**, 1056-1066.
5. Kirk, J. T. O., 1994: Light and photosynthesis in aquatic ecosystems, 2nd edition, Cambridge University Press, 509 pp.
6. Tanré, D., M. Herman, P.-Y. Deschamps, and A. De Lefte, 1979: Atmospheric modeling for space measurements of ground reflectances, including bi-directional properties. *Appl. Optics*, **18**, 3587-3594.
7. Young, D. F., P. Minnis, D. R. Doelling, G. G. Gibson, and T. Wong, 1998: Temporal interpolation methods for the clouds and Earth's Radiant Energy System (CERES experiment). *J. Appl. Meteor.*, **37**, 572-590.
8. Zege, E. P., A. P. Ivanov, and I. L. Katsev, 1991: Image transfer through a scattering medium. Springer-Verlag, New York, 349 pp.